

# Experimental quantum state transfer of an arbitrary single-qubit state on a cycle with four vertices using a coined quantum random walk

Gayatri Singh,<sup>1,\*</sup> Kavita Dorai,<sup>1,†</sup> and Arvind<sup>1,2,‡</sup>

<sup>1</sup>*Department of Physical Sciences, Indian Institute of Science Education & Research Mohali, Sector 81 SAS Nagar, Manauli PO 140306 Punjab India.*

<sup>2</sup>*Vice Chancellor, Punjabi University Patiala, 147002, Punjab, India*

We experimentally demonstrate the transfer of an unknown single-qubit state from Alice to Bob via a two-step discrete-time quantum random walk on a cycle with four vertices on a four-qubit nuclear magnetic resonance quantum processor. The qubits with Alice and Bob are used as coin qubits and the walk is carried out on in a two-qubit ‘Gaming Arena’. In this scheme, the required entangled state is generated naturally via conditional shift operators during the quantum walk, instead of being prepared in advance. We implement controlled operators at Bob’s end, which are controlled by Alice’s coin qubit and arena qubits, in order to reconstruct Alice’s randomly generated state at Bob’s end. To characterize the state transfer process, we perform quantum process tomography by repeating the experiment for a set of input states  $\{|0\rangle, |1\rangle, |+\rangle, |-\rangle\}$ . Using an entanglement witness, we certify that the quantum walk generates a genuine quadripartite entangled state of all four qubits. To evaluate the efficacy of the transfer scheme, We use quantum state tomography to reconstruct the transferred state by calculating the projection of the experimentally reconstructed four-qubit density matrix onto three-qubit basis states. Our results demonstrate that the quantum circuit is able to perform quantum state transfer via the two-step quantum random walk with high fidelity.

## I. INTRODUCTION

Quantum analogs of classical random walks are a versatile tool to perform quantum information processing tasks such as universal quantum computing [1], quantum search [2] and quantum simulation [3], and have been comprehensively reviewed in several articles [4–6]. Quantum walks have been experimentally implemented on several physical platforms such as nuclear magnetic resonance [7–9], trapped ions [10, 11], atoms in an optical lattice [12] and photonics [13, 14]. Quantum teleportation refers to sending an unknown quantum state between two parties, Alice and Bob, using classical information and quantum correlations [15–17]. Teleportation was first experimentally demonstrated using a pair of entangled photons [18], while later experiments used other physical platforms such as trapped ions [19], photonic qubits [20], liquid state nuclear magnetic resonance (NMR) [21], superconducting qubits [22], and nitrogen vacancy centers [23].

Standard quantum teleportation schemes require an entangled state to be shared *a priori* between the two parties and since in coined quantum random walks the conditional shift operator can introduce entanglement between the coin and position spaces, the question arose as to whether quantum random walks could be used for quantum teleportation. To resolve this question, a new scheme to perform teleportation of an unknown quantum state was designed which used two-step quantum

walks on a line and on a cycle with four vertices [24]. Two quantum walkers on different quantum structures such as a line, a cycle and two-vertices complete graphs with loops were used to teleport an arbitrary two-qubit state and were generalized to  $N$  walkers and  $N$ -qubit states [25–27]. Controlled quantum teleportation was proposed based on three-coin quantum random walks, where a conditional shift operator was used to generate entanglement between the position and coin spaces [28].

Experimental realizations of the quantum teleportation of an arbitrary two-qubit state using a four-qubit cluster state and of quantum teleportation using coined quantum walks were demonstrated on the IBM cloud quantum computing platform [29, 30]. An arbitrary two-qubit quantum-controlled teleportation scheme wherein the sender performs two Bell state measurements and the receiver performs a unitary operation to reconstruct the state was performed on an IBM quantum computer [31]. Perfect state transfer of entangled states by quantum walks with two coins was demonstrated on the IBM quantum experience [32].

In this work, we experimentally demonstrate the transfer of an unknown single-qubit quantum state between two parties (Alice and Bob), via a quantum random walk on a cycle with four vertices, on a four-qubit NMR quantum processor. Although previous quantum random walk schemes have been used to achieve quantum teleportation, we choose to instead use the scheme to achieve quantum state transfer. This is because our quantum processor of choice is based on liquid-state NMR, wherein the qubits are physically located on the same molecule, and it is hence natural to conceptualize the protocol as a state transfer instead of state teleportation. We recast the quantum random walk scheme as a two-player quantum game played by Alice and Bob in a two-qubit

---

\* [ph20015@iisermohali.ac.in](mailto:ph20015@iisermohali.ac.in)

† [kavita@iisermohali.ac.in](mailto:kavita@iisermohali.ac.in)

‡ [arvind@iisermohali.ac.in](mailto:arvind@iisermohali.ac.in)

‘Gaming Arena’, with Alice and Bob each having one coin qubit which they flip and use to play the game. The standard protocol to transfer an unknown quantum state via a two-step quantum random walk involves the generation of a shared entangled state during the walk, projective measurements which are performed by Alice and communicated to Bob via a classical channel, and finally a set of measurements that Bob performs based on Alice’s measurement outcomes. Since projective measurements are not possible on NMR quantum processors, while controlled operations between all the involved qubits are possible, we use unitary operations at Bob’s end which are controlled by Alice’s qubit and the Arena qubits, to achieve the state transfer. Our scheme uses conditional shift operators on the ‘Arena qubits’ in the ‘Gaming Arena’ to execute one step of the quantum walk. After Alice and Bob execute one step each of the quantum random walk by using their coin qubits, controlled operations are applied on Bob’s coin qubit, which then gets pushed into the randomly generated initial state of Alice’s coin qubit. This completes the quantum state transfer protocol. We note here that this scheme to transfer the state, which was randomly generated by Alice’s coin qubit, to Bob’s end is implementable only because all the four qubits (the two coin qubits as well as the two ‘Arena’ qubits) are all located within the same molecule. We use quantum process tomography to characterize the teleportation scheme, by repeating the experiment for a set of four different input states  $\{|0\rangle, |1\rangle, |+\rangle$  and  $|-\rangle\}$ . The tomographed four-qubit state contains information about four-qubit entanglement which is generated during the quantum walk. We use an entanglement witness to verify that the generated four-qubit state indeed has genuine quadripartite entanglement [33]. To verify that the state has indeed been transferred with high fidelity, we reconstruct the state by taking projections of the experimental four-qubit density matrix onto three-qubit basis states which are determined from Alice’s measurements. We are able to achieve near-complete transfer of the unknown quantum state with high fidelity. Our results also demonstrate the viability of our four-qubit NMR system as a robust and versatile quantum processor, which has good decoherence properties and a high degree of quantum control.

This paper is organized as follows: The basic theoretical framework is briefly reviewed in Section II, with a review of the coined discrete time quantum random walk and a description of how to accomplish transfer of an unknown single-qubit state by quantum random walks on a cycle with four vertices, contained in Sections II A and II B, respectively. Details of the experimental implementation of the teleportation protocol on an NMR quantum processor are given in Section III A. Section III B contains the details of the experimental settings and NMR pulse sequences, while Section III C contains a detailed analysis of the experimental results. Section IV contains a few concluding remarks.

## II. BASIC THEORETICAL FRAMEWORK

In this section, the basics of modeling a discrete time quantum random walk on four vertices using multiple coins as well as the protocol for transfer of an unknown single-qubit state using a quantum random walk will be discussed.

### A. Coined Quantum Random Walks on a Closed Cycle

A coined discrete time quantum random walk occurs in the joint space of position (in which the ‘walker’ walks) qubits and the coin (or coins) qubit(s). The total Hilbert space can be written as  $\mathcal{H} = \mathcal{H}_P \otimes \mathcal{H}_C$ , where  $\mathcal{H}_P$  is the Hilbert space of the walker and  $\mathcal{H}_C$  is the Hilbert space of the coin. At each step of the quantum walk, the coin is flipped, and then depending upon the state of the coin, the walker moves either in the clockwise or the anticlockwise direction. If the coin is in the state  $|0\rangle$ , the walker moves in the anticlockwise direction and if the coin is in the state  $|1\rangle$ , the walker moves in the clockwise direction. Since the quantum walk occurs over the closed topology of a cycle, the walker moves in the clockwise (anticlockwise) direction and not in the usual left(right) directions. For a coined quantum walk on a closed cycle denoted by a graph  $G(V, E)$  with edges  $E$  and vertices  $E$ , the Hilbert space  $H_v$  is spanned by the vertex states  $|v\rangle$ , where  $v \in V$  and the coin Hilbert space  $H_c$  is spanned by the qubit states  $\{|0\rangle, |1\rangle\}$ , with the total Hilbert space being given by  $H = H_v \otimes H_c$ . One step of the quantum walk is controlled by the unitary operator  $U = S(I \otimes C)$ , where  $C$  is the coin flipping operator and  $S$  is the conditional shift operator acting on  $H_v \otimes H_c$  which is defined as [24]:

$$S_{\pm} = |i \pm 1 \bmod n\rangle \langle i|$$

$$S = \sum_{i=0}^{n-1} (S_+ \otimes |0\rangle_c \langle 0| + S_- \otimes |1\rangle_c \langle 1|) \quad (1)$$

where  $n$  refers to the number of vertices on the cycle. We use a closed cycle with four vertices to implement a two-step quantum random walk, with each vertex denoting a possible position. The position qubits change their location depending on the outcome of the coin qubit after it is flipped. Without loss of generality, the coin operator  $C$  can be arbitrarily set to any single-qubit unitary, without affecting the outcome of the quantum walk [24].

### B. Transferring a Single-Qubit State on a Four-Cycle

Standard teleportation schemes begin with preparing an entangled state to be shared beforehand between the two parties. On the other hand, when using a quantum random walk to achieve teleportation, the entangled state

is generated by two conditional shift operators during the steps of the walk. Previous NMR experimental protocols to realize quantum teleportation were able to teleport the state of a nuclear spin “locally” from one atom to another, located physically on the same molecule. Since in the NMR scenario, the state is teleported to another location within the same molecule, it can be construed as not strictly being teleportation but as being akin to state transfer. We hence recast the entire theoretical scheme described in the Reference [24] in terms of achieving quantum state transfer instead of quantum teleportation. Consider a quantum random walk on a closed cycle with four vertices, involving two coins, one with Alice and the other with Bob. The protocol is designed to transfer the coin state of Alice to the coin state of Bob, and is similar in spirit to the quantum teleportation protocol. The protocol can be visualized as a two-player game that Alice and Bob play, with the quantum walk taking place in the space of the two ‘Arena Qubits’. The schematic of the two-player game is depicted in Figure 1. The ‘Arena’ space is spanned by the vertices and the coin space is spanned by the edges of the cycle. There are two directed edges at each vertex in Figure 1. Thus, the dimension of the ‘Arena’ space is four, while that of each of Alice’s and Bob’s coin space is two. Initially, Alice’s coin is prepared in an unknown random one-qubit state denoted by  $|\phi\rangle = a|0\rangle + b|1\rangle$  with  $|a|^2 + |b|^2 = 1$  in Figure 1. This amounts to preparing the entire system in the initial state  $|\psi_{\text{in}}\rangle = |00\rangle \otimes |\phi\rangle \otimes |0\rangle$ . Alice then uses her coin qubit  $A_c$ , to move one step in the random walk by using the shift operator (denoted by the box labeled  $W_1$  in Figure 1). Bob starts with his coin in a state which is prepared by applying a Hadamard gate on his qubit in the  $|0\rangle$  state, which is thus in an equal superposition of  $|0\rangle$  and  $|1\rangle$  states. Bob then executes the next step of the quantum random walk by using his coin and applying the conditional shift operator to the ‘Arena qubits’ in the game arena (denoted by the box labeled  $W_2$  in Figure 1). After that, controlled operations are applied to Bob’s coin qubit. Bob’s coin is thus pushed into the unknown random initial state of Alice. This step completes the implementation of the protocol. The conditional shift operator (Eq. (1)) becomes

$$S = (|0\rangle\langle 1| + |1\rangle\langle 2| + |2\rangle\langle 3| + |3\rangle\langle 0|) \otimes |1\rangle_{c_c}\langle 1| + (|0\rangle\langle 3| + |1\rangle\langle 0| + |2\rangle\langle 1| + |3\rangle\langle 2|) \otimes |0\rangle_{c_c}\langle 0| \quad (2)$$

Without loss of generality, the coin operator of Alice is chosen to be the Identity operation and the coin operator of Bob is chosen to be the Hadamard gate.

The state after the second step of the quantum walk evolves to:

$$|\psi\rangle_2 = \frac{1}{\sqrt{2}}(a|0001\rangle + b|1000\rangle + a|0110\rangle + b|1111\rangle) \quad (3)$$

Alice now perform measurements on her qubits: on the position qubit in the  $\{|0\rangle, |1\rangle\}$  basis and coin qubit in the  $\{|+\rangle, |-\rangle\}$  basis.

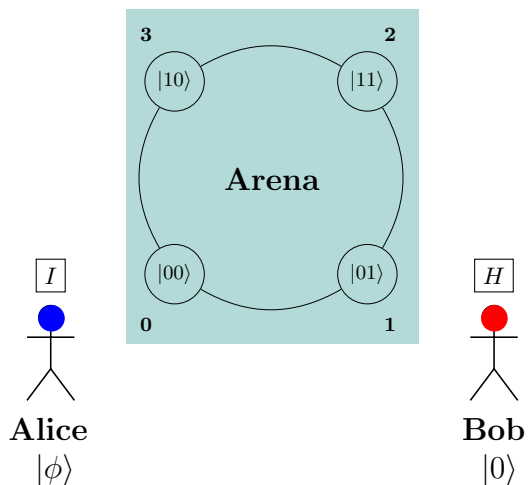


FIG. 1. The two-player ‘Game Arena’ is depicted by a closed cycle with four vertices (**0, 1, 2, 3**) representing the states  $|00\rangle, |01\rangle, |11\rangle$  and  $|10\rangle$ , respectively. Alice and Bob use their respective coin qubits to play the game and move from one vertex to another on the closed cycle. If the coin qubit is in the  $|0\rangle$  state, the move on the closed cycle is executed in the anticlockwise direction, and if it is in the  $|1\rangle$  state, the move is executed in the clockwise direction. Alice’s coin operator is the Identity  $I$  gate, while Bob’s coin operator is the Hadamard  $H$  gate. Alice begins the game with her coin in the randomly generated  $|\phi\rangle$  state, while Bob begins the game with his coin in the  $|0\rangle$  state.

Alice’s measurement outcomes and Bob’s corresponding controlled operations are given in Table I. After two steps of the quantum walk, a Hadamard gate is applied on Alice’s coin space so that Alice performs all measurements in the  $\{|0\rangle, |1\rangle\}$  basis. Thus, the state after two steps of the quantum walk is given by:

$$|\psi\rangle_f = \frac{1}{2}\{|000\rangle \otimes (a|1\rangle + b|0\rangle) + |100\rangle \otimes (a|1\rangle - b|0\rangle) + |011\rangle \otimes (a|0\rangle + b|1\rangle) + |111\rangle \otimes (a|0\rangle - b|1\rangle)\} \quad (4)$$

From the state  $|\psi\rangle_f$  (Eq. (4)), one observes that, if Alice’s position qubit is in the  $|00\rangle$  state and Alice’s coin qubit is in the  $|0\rangle$  state, Bob is required to apply a  $\sigma_x$  ( $X$ ) gate in order to recover the transferred state, and so on. After implementing the controlled operations listed in Table I, the state is given by:

$$|\Psi\rangle = \frac{1}{2}\{|000\rangle + |100\rangle + |011\rangle + |111\rangle\} \otimes (a|0\rangle + b|1\rangle) \quad (5)$$

Finally, by measuring Bob’s qubit, one can verify that the state  $|\phi\rangle = a|1\rangle + b|0\rangle$  has indeed been transferred from Alice to Bob.

The quantum circuit to experimentally realize the transfer of an unknown single-qubit state using a two-step quantum random walk on a cycle with four vertices is shown in Figure 2.  $A_c$  and  $B_c$  denote the coin qubits of Alice and Bob, respectively, while the other two qubits are denoted as the ‘Arena qubits’. The coin state of Alice

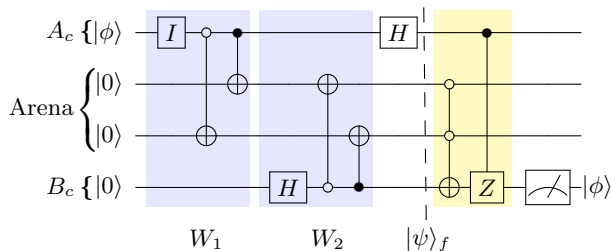


FIG. 2. Quantum circuit to transfer an unknown single-qubit state  $|\phi\rangle$  using a two-step quantum random walk on a cycle with four vertices.  $A_c$  and  $B_c$  denote the coin qubits of Alice and Bob, respectively, while the two middle qubits are labeled as the ‘Arena’ qubits.  $W_1$  and  $W_2$  denote the first and second steps of the quantum walk. The yellow shaded box represents the implementation of unitaries corresponding to the controlled operations.

is the randomly generated single-qubit state  $|\phi\rangle$ , which is transferred to the coin state of Bob, at the end of the circuit. The boxes labeled  $W_1$  and  $W_2$  contain the gates required to implement the first and second steps of the quantum walk;  $I$  and  $H$  and  $Z$  denote an Identity operator, a Hadamard gate, and a Pauli  $Z$  operator, respectively. The last yellow shaded in Figure 2 contains the gates required to implement the controlled operations given in Table I.

Measurement Results		Controlled Operation
$A_c$	Arena Qubits	$M$
0	11	$I$
1	11	$Z$
0	00	$X$
1	00	$ZX$

TABLE I. Measurement results on Alice’s coin qubit ( $A_c$ ) and the corresponding controlled operations  $M$  on Bob’s coin qubit ( $B_c$ );  $Z$  and  $X$  denote the Pauli matrices  $\sigma_z$  and  $\sigma_x$  respectively, while  $I$  is the Identity (‘do nothing’) operator.

### III. EXPERIMENTAL IMPLEMENTATION OF TELEPORTATION VIA A TWO-STEP QUANTUM RANDOM WALK

#### A. Experimental NMR Details

We used four  $^{13}\text{C}$  nuclei of the  $^{13}\text{C}$ -labeled trans-crotonic acid molecule dissolved in acetone- $\text{D}_6$  to physically realize four qubits. The molecular structure and system parameters including the chemical shifts  $\nu_i$ ,  $T_1$  and  $T_2$  relaxation times and the scalar J-coupling constants are given in Figure 3. All the experiments were performed at ambient temperature ( $\approx 300\text{K}$ ) on a Bruker DRX Avance III 600 MHz NMR spectrometer equipped with a standard 5 mm QXI probe. The methyl group

$C_1$	25185.31			
$C_2$	72.35	18519.58		
$C_3$	1.02	69.69	21815.48	
$C_4$	7.05	1.46	40.64	2561.66
T1	20.02	7.31	8.39	7.26
T2	2.34	1.32	1.12	1.22
	$C_1$	$C_2$	$C_3$	$C_4$

FIG. 3. Molecular structure and system parameters of  $^{13}\text{C}$ -labeled trans-crotonic acid with the four carbon atoms labeled as  $C_1, C_2, C_3, C_4$ . The diagonal elements in the table represent the chemical shifts (in Hz), while the off-diagonal elements are the J-couplings (in Hz) between two spins. The  $T_1$  and  $T_2$  relaxation times (in sec) are given in the last two rows of the table. Green and red balls represent oxygen and hydrogen atoms, respectively.

and other proton spins were decoupled throughout the experiments, via a composite pulse-based broadband decoupling sequence (WALTZ-16).

Under the weak coupling approximation, the NMR Hamiltonian for a four spin-1/2 system in the rotating frame is given by:

$$\mathcal{H} = - \sum_{i=1}^4 (\omega_i - \omega_{\text{rf}}) I_{iz} + \sum_{i<j,j=1}^4 2\pi J_{ij} I_{iz} I_{jz} \quad (6)$$

where  $i$  labels the spin,  $\omega_{\text{rf}}$  is the rotating frame frequency,  $\omega_i = 2\pi\nu_i$  and  $I_{iz}$  denote the Larmor frequency and the  $z$ -component of the spin angular momentum of the  $i$ th spin respectively, and  $J_{ij}$  is the strength of the scalar coupling between the  $i$ th and  $j$ th spins.

The system was initialized in a pseudopure state (PPS) using the spatial averaging method, with the density operator being given by [34, 35]:

$$\rho_{0000} = \frac{1 - \alpha}{2^4} \mathbb{I}_{16} + \alpha |0000\rangle\langle 0000| \quad (7)$$

where  $\mathbb{I}_{16}$  is the  $16 \times 16$  identity matrix and  $\alpha \sim 10^{-5}$  is the thermal spin polarization. The NMR pulse sequence using rf pulses,  $z$ -gradient pulses and time evolution periods used to prepare the  $\rho_{0000}$  PPS starting from thermal equilibrium is depicted in Figure 4 (upto the first dashed line). All the rf pulses were constructed using the GRAPE optimization technique [36, 37], which assembles a single shaped pulse from a large number of individually controlled short segments. All single-qubit GRAPE pulses were designed to be robust against rf inhomogeneity with a duration of around  $340 \mu\text{s} - 360 \mu\text{s}$  and an average fidelity  $\geq 0.997$ . Wherever possible, two or more

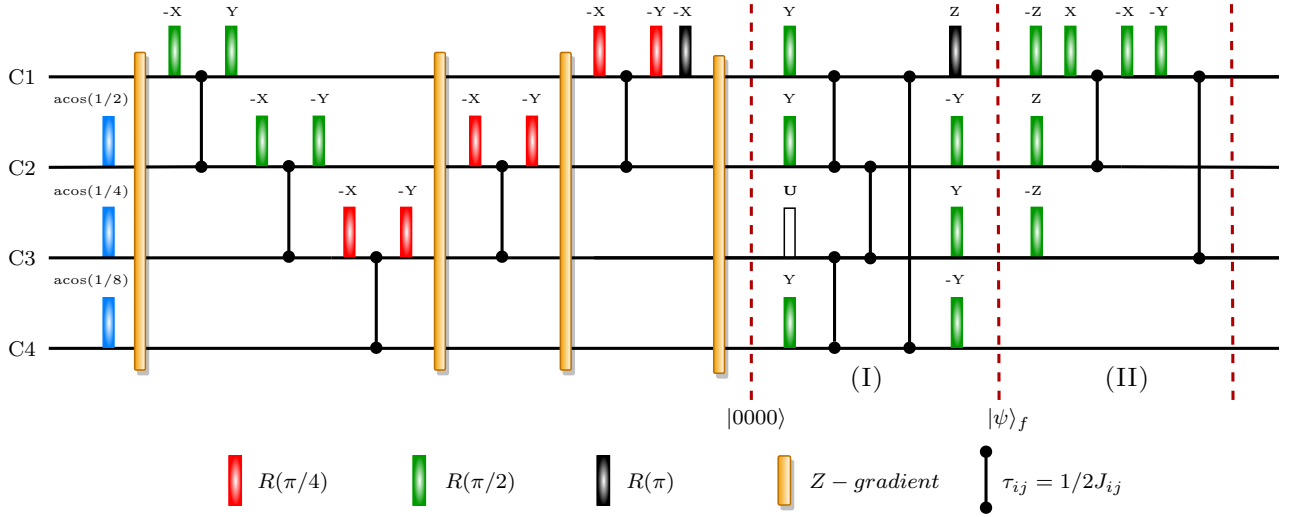


FIG. 4. NMR pulse sequence to implement the two-step quantum random walk circuit to achieve teleportation of an arbitrary single-qubit state  $|\phi\rangle$ . The sequence of rf pulses, z-gradients and time evolution periods upto the first dashed line prepares the system in the  $\rho_{0000}$  PPS, starting from thermal equilibrium. The sequence given in the box labeled I implements the two-step quantum walk, while the box labeled II implements the unitaries corresponding to the controlled operations. The phase of each rf pulse is given above each pulse bar;  $\tau_{ij} = \frac{1}{2J_{ij}}$  corresponds to the free evolution period and the unitary  $U$  is used to prepare the state  $|\phi\rangle$ ; the refocusing schemes are not depicted.

spin-selective rf pulses were combined and implemented via a single GRAPE pulse.

Constrained convex optimization based reduced state tomography [38, 39] was used to reconstruct valid experimental density matrices with a set of tomography operations [40–42]:

$$\{IIII, IIIX, XIIIX, XIIY, YYII, IXXY, IYXY, IYYY, XXXI, XYYI, YIXX, YYYI, XXXX, YXXX, YXYY\}$$

where  $I$  is the identity ('do nothing') operator and  $X(Y)$  are qubit-selective  $\pi/2$  rotations applied along the  $x(y)$  axis.

The fidelity of the experimentally reconstructed state as compared to the theoretically expected state was computed using the Uhlmann-Jozsa fidelity measure [43, 44]:

$$\mathcal{F}(\rho_{\text{expt}}, \rho_{\text{th}}) = \frac{|\text{Tr}[\rho_{\text{expt}}\rho_{\text{th}}^\dagger]|}{\sqrt{\text{Tr}[\rho_{\text{expt}}\rho_{\text{expt}}^\dagger]\text{Tr}[\rho_{\text{th}}\rho_{\text{th}}^\dagger]}} \quad (8)$$

where  $\rho_{\text{expt}}$  and  $\rho_{\text{th}}$  are the experimentally reconstructed and the theoretically expected density matrices, respectively. The  $|0000\rangle$  PPS was prepared with a total pulse sequence duration of  $\approx 41$  ms with an experimental fidelity  $0.9812 \pm 0.0020$ .

### B. Experimental Quantum State Transfer Using Revised Measurements

In order to implement the quantum transfer circuit, we denote the four carbons in the molecule according to the

notation:  $C_1$  is Bob's coin,  $C_3$  is Alice's coin and  $C_2, C_4$  are the Arena qubits (see Figure 3 for qubit labels).

The state  $|\psi\rangle_f$  (Eq 4) after two steps of the random walk is given by:

$$|\psi\rangle_f = \frac{1}{2}\{(a|0\rangle + b|1\rangle) \otimes |101\rangle + (a|0\rangle - b|1\rangle) \otimes |111\rangle + (a|1\rangle + b|0\rangle) \otimes |000\rangle + (a|1\rangle - b|0\rangle) \otimes |010\rangle\} \quad (9)$$

and the state  $|\Psi\rangle$  (Eq 5) is given by:

$$|\Psi\rangle = \frac{1}{2}\{|000\rangle + |010\rangle + |101\rangle + |111\rangle\} \otimes (a|0\rangle + b|1\rangle) \quad (10)$$

We decomposed the quantum circuit given in Figure 2 as a set of single-qubit rotations and  $J$ -coupling gates, using controlled-NOT gates (not shown in the Figure). The corresponding NMR pulse sequence is shown in the dashed regions I and II in Figure 4. This particular sequence is efficient because of the cancellation of certain terms in the NMR pulse decomposition of these unitaries due to spin angular momentum commutation rules. We designed gate implementation under simultaneous evolution of all the  $J$ -couplings, using the refocusing method described in Reference [35], which finds an optimal solution for the required interactions using a MATLAB program with the in-built *linprog* function. In our case, we found an optimal solution with 9 time periods and 10 refocusing pulses for simultaneous evolution under the required scalar  $J$ -couplings  $J_{12}, J_{23}, J_{34}$  and  $J_{14}$ , with a total implementation time of 82.19 ms, which is 18.2% shorter than the unoptimized implementation time of 97.12 ms.

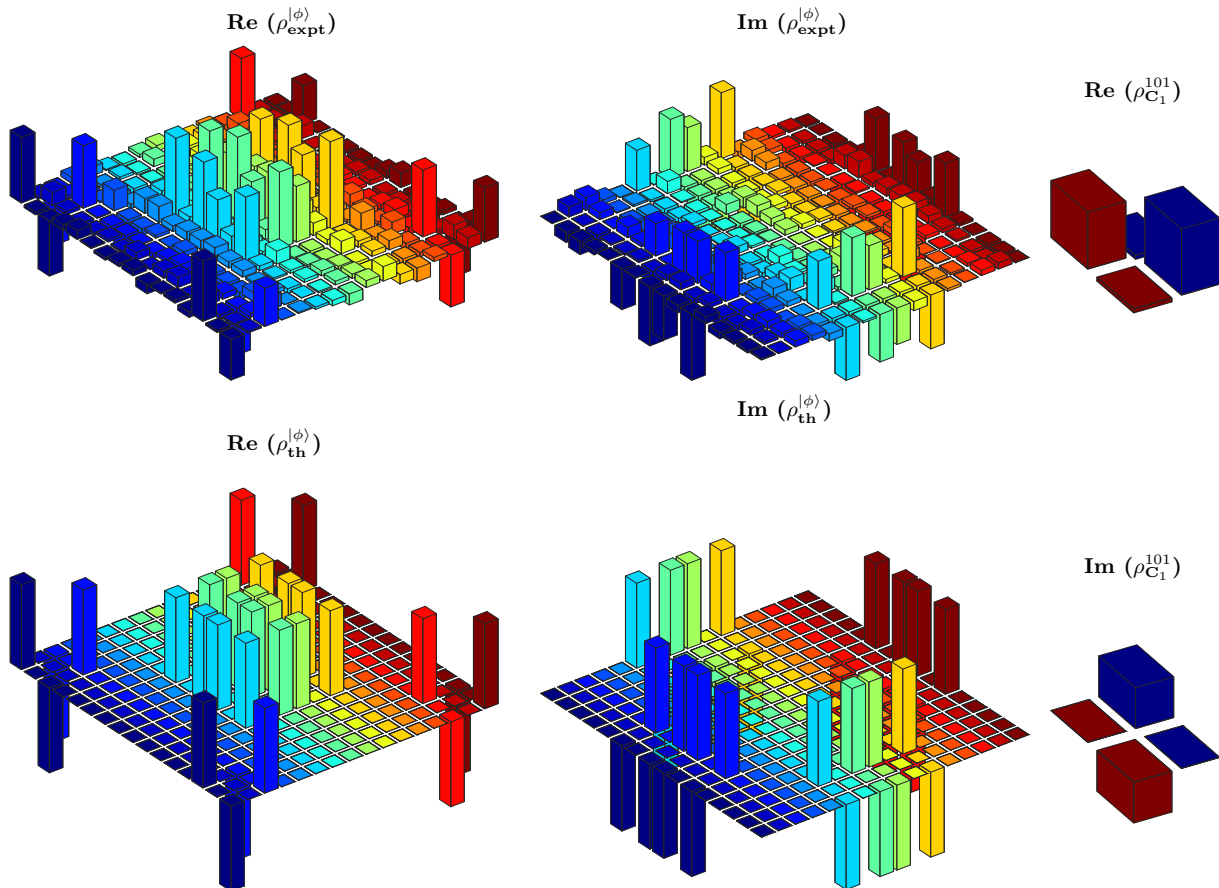


FIG. 5. Real (left) and imaginary (right) parts of the experimentally tomographed and the theoretically expected four-qubit state  $\rho_{\text{expt}}^{|\phi\rangle} = |\psi\rangle_f \langle\psi|$  for the input state  $|\phi\rangle = |-\rangle$ , with a fidelity of  $0.9183 \pm 0.0028$ . The tomographs in the right-most column show the real and imaginary parts of the teleported state reconstructed at Bob's qubit  $\rho_{C_1}^{101}$ , with a fidelity of  $0.9785 \pm 0.002$ .

Furthermore, using this refocusing method and GRAPE optimization, the evolution time of the coupling  $J_{13}$  is dramatically reduced from  $\sim 490$  ms to  $\sim 25$  ms. Our numerically optimized pulse sequence shortens the duration of the overall pulse sequence as well as reduces the number of pulses used for refocusing, thus mitigating the undesirable effects of decoherence. All the pulses including the refocusing pulses were designed using the GRAPE optimization algorithm with a fidelity  $\geq 0.998$  and are robust against rf inhomogeneity [45]. All the pulses corresponding to single-qubit rotations have a duration of  $\approx 340 - 360 \mu\text{s}$ .

The complete NMR pulse sequence shown in Figure 4 was implemented, with a total time duration of  $\sim 156$  ms. We note here that the measurement outcomes of the Arena qubits are either 00 or 11 (Table I). In case the Arena qubits are in the  $|11\rangle$  state, no further operation is required. However, if they are in the  $|00\rangle$  state, the corresponding controlled unitary operation becomes a NOT gate on Bob's qubit, which is equivalent to implementing a Toffoli gate with zero control. Since both qubits are in the  $|0\rangle$  state, we considered the control only from one qubit. Hence, to simplify the experimental scheme, in-

stead of implementing the zero-controlled Toffoli gate, we implemented an equivalent 'zero-controlled-CNOT' gate.

After implementing the entire pulse sequence, only Bob's qubit ( $C_1$ ) is tomographed in order to reconstruct the transferred state. This experimental scheme is efficient in terms of the number of experiments, as it requires only two tomography pulses *IIII* and *XIII* to reconstruct the state. In order to evaluate the efficiency of the scheme, we performed the experiment for a set of four different input states  $|\phi\rangle = \{|0\rangle, |1\rangle, |+\rangle, |-\rangle\}$ .

The experimentally reconstructed transferred state for the input state  $|\phi\rangle = |-\rangle$  is shown in Figure 6. The average experimental fidelities for the input states  $|0\rangle, |1\rangle, |+\rangle$  and  $|-\rangle$  are  $0.9918 \pm 0.0006$ ,  $0.9924 \pm 0.0012$ ,  $0.96 \pm 0.0027$  and  $0.9896 \pm 0.0007$ , respectively. These high state fidelities are a testimony to the fact that the experimental scheme is well able to transfer the desired single-qubit state.

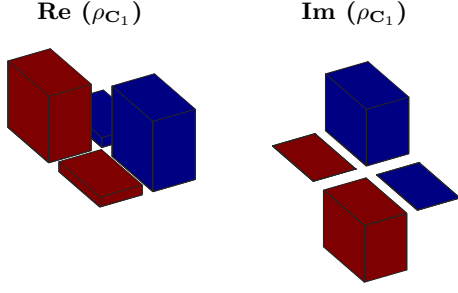


FIG. 6. Real (left) and imaginary (right) parts of the experimentally tomographed transferred state at Bob's qubit  $\rho_{C_1}$  with a fidelity of  $0.9896 \pm 0.0007$  for the input state  $|\phi\rangle = |-\rangle$ .

### C. Verifying the Fidelity of the Transferred State

We also wanted to independently verify the efficacy of the transfer protocol by reconstructing the state which has been transferred to Bob and computing its fidelity. We hence repeated the experimental protocol for a set of different input states  $|\phi\rangle = \{|0\rangle, |1\rangle, |+\rangle, |-\rangle\}$ , where  $|+\rangle = \frac{|0\rangle+|1\rangle}{2}$  and  $|-\rangle = \frac{|0\rangle+i|1\rangle}{2}$ . The NMR pulse sequence after PPS preparation and including the box I (Figure 4) is applied with a total gate implementation time of  $\sim 124$  ms. The density matrix of the four-qubit entangled state  $\rho_{\text{expt}}$  is reconstructed using quantum state tomography. The real and imaginary parts

of the theoretically expected and experimentally reconstructed four-qubit density matrix for the input state  $|\phi\rangle = |-\rangle$  are shown in Figure 5.

We analyzed this experimentally reconstructed four-qubit density matrix to obtain the transferred state. It is to be noted that the measurement outcomes of Alice's qubits do not contain any information about the input state  $|\phi\rangle$ . However, one can retrieve the input state at Bob's qubit from the results of Alice's measurements. To achieve this, we calculated the projections of  $\rho_{\text{expt}}$  onto the basis states  $|C_2C_3C_4\rangle = |ijk\rangle = \{|000\rangle, |010\rangle, |101\rangle, |111\rangle\}$  [22]. The qubits  $C_2, C_3$  and  $C_4$  are then traced over and the state of Bob's qubit  $\rho_{C_1}^{ijk}$  is reconstructed by renormalizing the reduced density matrix and applying suitable controlled operations  $M$  listed in Table I:

$$\sigma_{C_1}^{ijk} = \frac{\text{Tr}_{C_2C_3C_4}[P_{ijk}\rho_{\text{expt}}P_{ijk}^\dagger]}{\text{Tr}[P_{ijk}\rho_{\text{expt}}]}$$

$$\rho_{C_1}^{ijk} = M \cdot \sigma_{C_1}^{ijk} \cdot M^\dagger \quad (11)$$

where  $P_{ijk} = I \otimes |ijk\rangle\langle ijk|$  are projectors. Figure 5 depicts the real and imaginary parts of the experimentally reconstructed state  $\rho_{C_1}^{101}$  and the theoretically expected state respectively, for which the controlled operation  $M$  is identity. The fidelities of the four-qubit state  $\rho_{\text{expt}}$  and the reconstructed state of Bob's qubit corresponding to the different input states  $|\phi\rangle = |0\rangle, |1\rangle, |+\rangle$  and  $|-\rangle$ , are given in Table II.

Input State $ \phi\rangle$	Fidelity of Four-Qubit State ( $\rho_{\text{expt}}$ )		Fidelity of Bob's Reconstructed State		
		$\rho_{C_1}^{101}$	$\rho_{C_1}^{111}$	$\rho_{C_1}^{000}$	$\rho_{C_1}^{010}$
$ 0\rangle$	$0.9162 \pm 0.0025$	$0.9632 \pm 0.0022$	$0.9863 \pm 0.0008$	$0.9906 \pm 0.006$	$0.9651 \pm 0.0036$
$ 1\rangle$	$0.9180 \pm 0.0068$	$0.9809 \pm 0.0049$	$0.9550 \pm 0.0057$	$0.9943 \pm 0.0013$	$0.9384 \pm 0.0013$
$ +\rangle$	$0.9357 \pm 0.0018$	$0.9880 \pm 0.0014$	$0.9928 \pm 0.0011$	$0.9891 \pm 0.0025$	$0.9775 \pm 0.0015$
$ -\rangle$	$0.9183 \pm 0.0028$	$0.9785 \pm 0.002$	$0.9527 \pm 0.0082$	$0.9712 \pm 0.0081$	$0.9666 \pm 0.003$

TABLE II. Fidelities of the experimentally prepared four-qubit state  $\rho_{\text{expt}}$  and the reconstructed state of Bob's qubit  $\rho_{C_1}^{ijk}$  ( $ijk = 101, 111, 000$  and  $010$ ), for different input states  $|\phi\rangle$ .

It is evident that the four-qubit entangled state  $|\psi\rangle_f$  is a cluster state [46, 47] under local unitary operations for input states  $|\pm\rangle$ , while it remains biseparable for input states  $|0\rangle$  and  $|1\rangle$ . We use a witness operator  $\mathcal{W}_{|\psi\rangle} = \frac{1}{2}I - |\psi\rangle\langle\psi|$  [33], to certify the presence of genuine quadripartite entanglement in  $\rho_{\text{expt}}$ . The factor of  $\frac{1}{2}$  in the expression for the witness operator  $\mathcal{W}_{|\psi\rangle}$  is the maximum possible fidelity between any biseparable state and  $|\psi\rangle$ . This ensures that if  $\text{Tr}[\mathcal{W}_{|\psi\rangle}\rho] < 0$ , the given state  $\rho$  has genuine four-qubit entanglement, while it is biseparable if  $\text{Tr}[\mathcal{W}_{|\psi\rangle}\rho] \geq 0$ . For the input state

$|+\rangle$ ,  $\text{Tr}[\mathcal{W}_{|\psi\rangle_f}\rho_{\text{expt}}] = -0.4358 \pm 0.0018$  and for the input state  $|-\rangle$ ,  $\text{Tr}[\mathcal{W}_{|\psi\rangle_f}\rho_{\text{expt}}] = -0.4183 \pm 0.0028$ , which clearly indicates the presence of genuine quadripartite entanglement.

We performed constrained convex optimization based quantum process tomography [38] to fully characterize the state transfer protocol. One can represent a completely positive map  $\rho_\phi = |\phi\rangle\langle\phi|$  with a quantum state  $\phi$ , which is to be transferred. In the operator sum repre-

sentation, the transfer process is defined as [48]:

$$\mathcal{E}(\rho_\phi) = \rho_{C_1}^{ijk} = \sum_{m,n=1}^{d^2} \chi_{mn}^{ijk} E_m \rho_\phi E_n^\dagger \quad (12)$$

where  $d$  is the dimension of the Hilbert space,  $E_m$  refers to the Pauli operator basis  $\{I, \sigma_x, \sigma_y, \sigma_z\}$  and  $\chi_{mn}^{ijk} = \sum_\alpha a_{\alpha m} a_{\alpha n}^*$  is the process matrix, which is a positive Hermitian matrix and satisfies the trace-preserving constraint  $\sum_{mn} \chi_{mn}^{ijk} E_n^\dagger E_m = I$ . Figure 7 shows the tomographed process matrices  $\chi^{ijk}$  which verify the expected unitary controlled operations listed in Table I. The fidelity of the experimentally reconstructed process matrix  $\chi_{\text{expt}}^{ijk}$  with respect to the theoretically expected process matrix  $\chi_{\text{th}}^{ijk}$  is calculated using the measure [49]:

$$\mathcal{F}^{ijk} = \frac{|\text{Tr}[\chi_{\text{expt}}^{ijk} \chi_{\text{th}}^{ijk\dagger}]|}{\sqrt{\text{Tr}[\chi_{\text{expt}}^{ijk} \chi_{\text{expt}}^{ijk\dagger}] \text{Tr}[\chi_{\text{th}}^{ijk} \chi_{\text{th}}^{ijk\dagger}]}} \quad (13)$$

The corresponding process fidelities for different projections are  $\mathcal{F}^{101} = 0.9682 \pm 0.0021$ ,  $\mathcal{F}^{111} = 0.9658 \pm 0.0015$ ,  $\mathcal{F}^{000} = 0.9842 \pm 0.0023$ , and  $\mathcal{F}^{010} = 0.9450 \pm 0.0015$ .

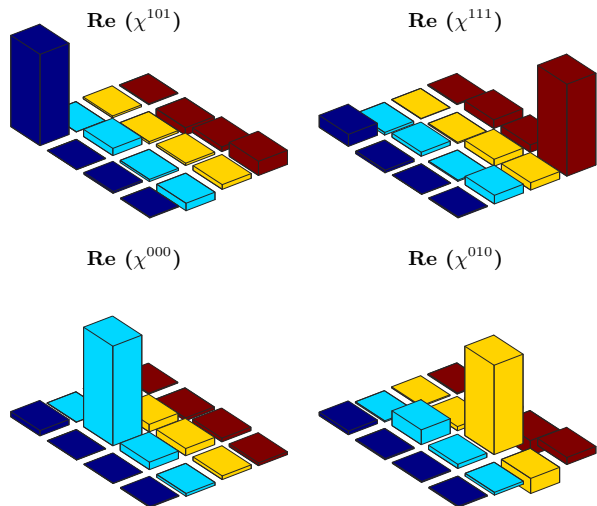


FIG. 7. Real parts of the experimentally tomographed process matrix  $\chi$  for different projections of  $\rho_{\text{expt}}$  onto the basis states  $|000\rangle$ ,  $|010\rangle$ ,  $|101\rangle$  and  $|111\rangle$ .

Our results lead to the conclusion that the experimental scheme is able to achieve almost perfect transfer of an arbitrary single-qubit state with high fidelity. We note here that for the NMR implementation of the state transfer scheme given in Figure 2, we have replaced single-shot readout [50] and real-time feedback [51] required for state transfer, with controlled unitary operations based on Alice's measurement outcomes. These controlled unitaries posed a significant experimental challenge since some J

couplings between qubits in the molecule chosen for the experiments are of a very weak strength. This implies that the corresponding gate times are rather long, increasing the likelihood of decoherence adversely affecting the computation, thereby leading to lower fidelities of the transferred state. For instance, the total time to naively implement the teleportation circuit for weakly coupled qubits C1 and C3 ( $J_{13} \approx 1.02$  Hz) was around  $490\mu\text{s}$ ; using specially crafted and GRAPE-optimized pulses we were able to dramatically reduce the experimental implementation time to around  $25\mu\text{s}$ . This allowed us to experimentally implement the state transfer protocol with high fidelity.

#### IV. CONCLUSIONS

We experimentally demonstrated a quantum state transfer scheme between two parties, Alice and Bob, using a two-step quantum walk on a cycle with four vertices. We performed constrained convex optimization based quantum state tomography and reconstructed the experimental density matrix. The creation of genuine quadripartite entanglement during the quantum walk was verified by using an entanglement witness. The transferred state was reconstructed on Bob's qubit by calculating its projection onto the basis states of Alice's qubit. Quantum process tomography was also performed to characterize the process matrix of the state transfer protocol, and only Bob's qubit was measured in order to reconstruct the transferred state. The scheme was able to achieve near perfect transfer of an arbitrary single-qubit state, with high state fidelity. Furthermore, the experimental circuit along with a few local unitaries can be used to generate four-qubit cluster states, which are of much interest in quantum information processing.

Our experimental schemes are general and can be easily extended to transferring states of a larger qubit register size via multi-coin, multi-walker setups. Our results demonstrate that coined quantum random walk schemes can be used to achieve robust transfer of an arbitrary quantum state and pave the way for wider applications in quantum communication and quantum information processing.

#### ACKNOWLEDGMENTS

All experiments were performed on a Bruker Avance-III 600 MHz FT-NMR spectrometer at the NMR Research Facility at IISER Mohali. Arvind acknowledges funding from the Department of Science and Technology (DST), India, Grant No:DST/ICPS/QuST/Theme-1/2019/Q-68. K.D. acknowledges funding from the Department of Science and Technology (DST), India, Grant No:DST/ICPS/QuST/Theme-2/2019/Q-74. G.S. acknowledges University Grants Commission (UGC), India, for financial support.



- 
- [1] A. M. Childs, *Phys. Rev. Lett.* **102**, 180501 (2009).
- [2] N. Shenvi, J. Kempe, and K. B. Whaley, *Phys. Rev. A* **67**, 052307 (2003).
- [3] P. Rebentrost, M. Mohseni, I. Kassal, S. Lloyd, and A. Aspuru-Guzik, *New J. Phys.* **11**, 033003 (2009).
- [4] A. Ambainis, *Int. J. Quantum Inf.* **01**, 507 (2003).
- [5] V. M. Kendon, *Philosophical Transactions of the Royal Society A: Mathematical, Physical and Engineering Sciences* **364**, 3407 (2006).
- [6] S. E. Venegas-Andraca, *Quant. Inf. Proc.* **11**, 1015 (2012).
- [7] J. Du, H. Li, X. Xu, M. Shi, J. Wu, X. Zhou, and R. Han, *Phys. Rev. A* **67**, 042316 (2003).
- [8] C. A. Ryan, M. Laforest, J. C. Boileau, and R. Laflamme, *Phys. Rev. A* **72**, 062317 (2005).
- [9] D. Lu, J. Zhu, P. Zou, X. Peng, Y. Yu, S. Zhang, Q. Chen, and J. Du, *Phys. Rev. A* **81**, 022308 (2010).
- [10] P. Xue, B. C. Sanders, and D. Leibfried, *Phys. Rev. Lett.* **103**, 183602 (2009).
- [11] F. Zähringer, G. Kirchmair, R. Gerritsma, E. Solano, R. Blatt, and C. F. Roos, *Phys. Rev. Lett.* **104**, 100503 (2010).
- [12] M. Genske, W. Alt, A. Steffen, A. H. Werner, R. F. Werner, D. Meschede, and A. Alberti, *Phys. Rev. Lett.* **110**, 190601 (2013).
- [13] M. A. Broome, A. Fedrizzi, B. P. Lanyon, I. Kassal, A. Aspuru-Guzik, and A. G. White, *Phys. Rev. Lett.* **104**, 153602 (2010).
- [14] A. Peruzzo, M. Lobino, J. C. F. Matthews, N. Matsuda, A. Politi, K. Poulios, X.-Q. Zhou, Y. Lahini, N. Ismail, K. Wörhoff, Y. Bromberg, Y. Silberberg, M. G. Thompson, and J. L. O'Brien, *Science* **329**, 1500 (2010).
- [15] C. H. Bennett, G. Brassard, C. Crépeau, R. Jozsa, A. Peres, and W. K. Wootters, *Phys. Rev. Lett.* **70**, 1895 (1993).
- [16] H.-J. Briegel, W. Dür, J. I. Cirac, and P. Zoller, *Phys. Rev. Lett.* **81**, 5932 (1998).
- [17] D. Gottesman and I. L. Chuang, *Nature* **402**, 390 (1999).
- [18] D. Bouwmeester, J.-W. Pan, K. Mattle, M. Eibl, H. Weinfurter, and A. Zeilinger, *Nature* **390**, 575 (1997).
- [19] M. D. Barrett, J. Chiaverini, T. Schaetz, J. Britton, W. M. Itano, J. D. Jost, E. Knill, C. Langer, D. Leibfried, R. Ozeri, and D. J. Wineland, *Nature* **429**, 737 (2004).
- [20] X.-M. Jin, J.-G. Ren, B. Yang, Z.-H. Yi, F. Zhou, X.-F. Xu, S.-K. Wang, D. Yang, Y.-F. Hu, S. Jiang, T. Yang, H. Yin, K. Chen, C.-Z. Peng, and J.-W. Pan, *Nat. Photonics* **4**, 376 (2010).
- [21] M. A. Nielsen, E. Knill, and R. Laflamme, *Nature* **396**, 52 (1998).
- [22] M. Baur, A. Fedorov, L. Steffen, S. Philipp, M. P. da Silva, and A. Wallraff, *Phys. Rev. Lett.* **108**, 040502 (2012).
- [23] W. Pfaff, B. J. Hensen, H. Bernien, S. B. van Dam, M. S. Blok, T. H. Taminiau, M. J. Tiggelman, R. N. Schouten, M. Markham, D. J. Twitchen, and R. Hanson, *science* **345**, 532 (2014).
- [24] Y. Wang, Y. Shang, and P. Xue, *Quant. Inf. Proc.* **16**, 221 (2017).
- [25] H.-J. Li, X.-B. Chen, Y.-L. Wang, Y.-Y. Hou, and J. Li, *Quantum Information Processing* **18**, 266 (2019).
- [26] T. Yamagami, E. Segawa, and N. Konno, *Quantum Information Processing* **20**, 224 (2021).
- [27] H.-J. Li, J. Li, and X. Chen, *Quantum Information Processing* **21**, 387 (2022).
- [28] W.-M. Shi, M.-X. Bai, Y.-H. Zhou, and Y.-G. Yang, *Quantum Information Processing* **22**, 34 (2022).
- [29] Y. Chatterjee, V. Devrari, B. K. Behera, and P. K. Panigrahi, *Quant. Inf. Proc.* **19**, 31 (2019).
- [30] S. Rajiuddin, A. Baishya, B. K. Behera, and P. K. Panigrahi, *Quantum Information Processing* **19**, 87 (2020).
- [31] X.-F. Liu, D.-F. Li, Y.-D. Zheng, X.-L. Yang, J. Zhou, Y.-Q. Tan, and M.-Z. Liu, *Chinese Physics B* **31**, 050301 (2022).
- [32] Y. Shang and M. Li, *Quantum Science and Technology* **5**, 015005 (2019).
- [33] Y. Tokunaga, T. Yamamoto, M. Koashi, and N. Imoto, *Phys. Rev. A* **74**, 020301 (2006).
- [34] A. Singh, K. Dorai, and Arvind, *Quantum Information Processing* **17**, 334 (2018).
- [35] G. Bhole, *Coherent control for quantum information processing*, Ph.D. thesis, Oxford U. (2020).
- [36] N. Khaneja, T. Reiss, C. Kehlet, T. Schulte-Herbrüggen, and S. J. Glaser, *J. Magn. Reson.* **172**, 296 (2005).
- [37] C. A. Ryan, C. Negrevergne, M. Laforest, E. Knill, and R. Laflamme, *Phys. Rev. A* **78**, 012328 (2008).
- [38] A. Gaikwad, Arvind, and K. Dorai, *Quant. Inf. Proc.* **20** (2021), 10.1007/s11128-020-02930-z.
- [39] A. Gaikwad, K. Shende, Arvind, and K. Dorai, *Scientific Reports* **12**, 3688 (2022).
- [40] J. Li, S. Huang, Z. Luo, K. Li, D. Lu, and B. Zeng, *Phys. Rev. A* **96**, 032307 (2017).
- [41] H. Singh, Arvind, and K. Dorai, *Physics Letters A* **380**, 3051 (2016).
- [42] H. Singh, Arvind, and K. Dorai, *Phys. Rev. A* **97**, 022302 (2018).
- [43] A. Uhlmann, *Rep. Math. Phys.* **9**, 273 (1976).
- [44] R. Jozsa, *J. Mod. Optics* **41**, 2315 (1994).
- [45] S. Dogra, A. Dorai, and K. Dorai, *International Journal of Quantum Information* **13**, 1550059 (2015).
- [46] R. Raussendorf and H. J. Briegel, *Phys. Rev. Lett.* **86**, 5188 (2001).
- [47] S. Muralidharan and P. K. Panigrahi, *Phys. Rev. A* **78**, 062333 (2008).
- [48] A. Gaikwad, D. Rehal, A. Singh, Arvind, and K. Dorai, *Phys. Rev. A* **97**, 022311 (2018).
- [49] A. Gaikwad, Arvind, and K. Dorai, *Quant. Inf. Proc.* **21**, 388 (2022).
- [50] F. Mallet, F. R. Ong, A. Palacios-Laloy, F. Nguyen, P. Bertet, D. Vion, and D. Esteve, *Nature Physics* **5**, 791 (2009).
- [51] A. C. Doherty and K. Jacobs, *Phys. Rev. A* **60**, 2700 (1999).